Modeling of drop sizes from effervescent atomization of gelatinized starch suspensions

J. Schröder[*1], M. Schlender[1], P. E. Sojka[2], V. Gaukel[1], H. P. Schuchmann[1]
[1]Food Process Engineering,
Karlsruhe Institute of Technology, Karlsruhe, Germany
[2]Maurice J. Zucrow Laboratories,
Purdue University, West Lafayette, IN, USA

Abstract

The applicability of previously published models for prediction of representative drop sizes resulting from effervescent atomization has been evaluated for usage with gelatinized starch suspensions. The calculated results are in qualitative agreement with experimental ones, but show an over prediction and reduced sensitivity to material properties. Analysis of the models shows that the material properties are neglected in a significant step.

Introduction

Effervescent atomization is a type of air-assisted atomization which is distinct in the formation of a two-phase flow prior to atomization [1], and has been investigated by several research groups. Some special types of the effervescent atomizer have been patented [2].

Effervescent atomization is a promising method for atomization of higher viscous and viscoelastic liquids as atomizing gas flow consumption is lower compared to the use of conventional external mixing nozzles [3]. A scheme describing the effervescent atomization process is shown in figure 1.

The goal of our ongoing investigation is to evaluate the applicability of effervescent atomization for gelatinized starch suspensions and later for spray drying these fluids. In the case of spray drying, the width of the spray drop size distribution is as important a characteristic quantity as the mean drop size. Too small drops can lead to thermal degradation reactions within the fine fraction while too large drops may lead to an incomplete drying of the coarse fraction at the same time.

The focus of the present work is the evaluation of existing models for prediction of representative drop sizes for these fluids [4],[5]. There have been several investigations on the prediction of drop size distributions [6] but in this work only those which cover the prediction of a representative drop size where considered. All are based on material properties and atomization parameters, and allow simple calculation of the representative drop sizes without the need of vast computing power. Related work has been recently published treating secondary drop breakup in effervescent atomization utilizing computational fluid dynamic simulations [7].

Materials and Methods

The models published by *Lund et al.* [5] and *Geckler et al.* [4] are based on an ideal model of the atomization process which is separated into two calculation steps. It is assumed for the first calculation step that the two-phase mixture forms an annular flow in the nozzle exit orifice (see figure 1 middle and right) where the filament sheath consists of only liquid. Calculation of the liquid sheath thickness, t_F, is based on the nozzle outlet diameter, d_O, air to liquid ratio by mass, *ALR*, fluid densities and the air and liquid velocity slip ratio, *sr*. Since the velocities of air and liquid could not be measured from these experiments an iterative calculation method of *Ishii* [8] for the slip ratio and the void fraction, α, is used. See equations 1 and 2.

$$sr = \frac{v_a}{v_l} = \sqrt{\frac{\rho_l}{\rho_a}} \cdot \sqrt{\frac{\sqrt{\alpha}}{1+75\cdot(1-\alpha)}} \tag{1}$$

$$\alpha = \frac{1}{1+\frac{\rho_a \cdot sr}{\rho_l \cdot ALR}} \tag{2}$$

The slip ratio is used to calculate the air core diameter, d_A, according to equation 3 and from there the thickness of the surrounding liquid filament sheath is computed using equation 4.

* Corresponding author: jewe.schroeder@kit.edu

$$d_A = \sqrt{\frac{\rho_l \cdot ALR \cdot d_O^2}{\rho_l \cdot ALR + \rho_a \cdot sr}} \tag{3}$$

$$t_F = d_O - d_A \tag{4}$$

The cross section of the filament sheath is partitioned into a certain number of circles where the diameter equals the thickness of the filament sheath as shown in figure 1 right. The cross sectional area of the filament sheath is then divided by this number of circles. Finally, the diameter of a circle with the same area is calculated as shown in equation 5 and defined as the ligament diameter d_L.

$$d_L = \frac{2 \cdot (d_O - d_A)}{\sqrt{\pi}} \tag{5}$$

The second step of the calculation is based on a stability analysis of ligament fragmentation. The optimal wave length for ligament break-up is calculated according to *Weber* [9] with consideration of the interfacial tension and rheological properties. Low shear viscosity is used due to the assumption that the ligament breakup occurs in air moving at about the same velocity. The resulting drop size is calculated from the volume of the resulting ligament according to equation 6 and is defined in the present work as a representative drop size, x_{rep}. *Lund et al.* and *Geckler et al.* equated x_{rep} with the Sauter mean diameter $x_{1,2}$.

$$x_{rep} = \left[\frac{3}{2} \cdot d_L^3 \cdot \sqrt{2} \cdot \pi \cdot \sqrt{1 + \frac{3 \cdot \eta_L}{\sqrt{\rho_L \cdot \sigma_L \cdot d_L}}} \right]^{1/3} \tag{6}$$

Further it is assumed for liquids with elastic properties that no secondary drop breakup occurs. Gelatinized starch suspensions exhibit in dependency on concentrations significant elastic properties. Consequently, no secondary drop breakup was considered in the present work.

For the present experimental work, suspensions of water and gelatinized native corn starch (CS) or native waxy corn starch (WCS) were used in the weight percentages shown in table 1. In order to gelatinize the starch suspensions, they were heated in a closed vessel to 75 °C and kept at this temperature for 15 min while being stirred constantly with a propeller mixer.

The volume flow of atomizing gas and liquid fed to the nozzle were monitored using rotameters. The data were used for calculation of the *ALR*. Feed pressures of atomizing gas and liquid were read from analog gauges.

Drop size distributions were acquired using a Sympatec Helos/Vario KF laser diffraction sizing system with a lens covering 9,0 to 1750 µm. Measurements were made 250 mm from the nozzle exit orifice. Sauter mean diameters were calculated from the measured drop size distributions. High speed videos were taken at 20 kHz to investigate stability and near nozzle structure of the spray.

Surface tensions of the fluids were determined via a Wilhelmy-plate with a DataPhysics DCAT 21 tensiometer. Shear viscosities, η, of the CS suspensions were measured using a cone-plate geometry. Rotational rheometry measurements were made using a Haake Mars II. Due to the presence of a significant yield stress rotational rheometry measurements were not possible for the WCS suspensions. Here, complex viscosities, $|\eta^*|$, were measured using cone-plate geometry and oscillating measurements were made using a Haake Rheostress RS 150 rheometer. The measurement data are summarized in table 1.

Results and Discussion

The experimental characteristic drop size initially chosen for comparison with calculated representative drop size was the Sauter mean diameter. The representative drop sizes computed according to the calculation published by *Lund et al.* and *Geckler et al.* significantly over predict the experimentally determined Sauter mean diameters (see figure 2; x_{rep} orig.). A thorough revision of the calculation disclosed an error in the steps leading to equation 5, which resulted in a doubling of the ligament diameter. The error seems to be caused by the wrong calculation of the filament thickness displayed in equation 4. This was corrected as shown in equation 7 and 8.

$$t_F = \frac{d_O - d_A}{2} \qquad \equiv \textit{corrected equation (4)} \tag{7}$$

$$d_L = \frac{d_O - d_A}{\sqrt{\pi}} \qquad \equiv \textit{corrected equation (5)} \tag{8}$$

The drop sizes computed according to the corrected calculation of *Geckler et al.* better fit the experimental data for both CS and WCS, as can also be seen in figure 2 (x_{rep} corr.). Still, deviations between experimental and calculated data depict the need for model improvement. In the case of CS, the spread of the experimental Sauter mean diameters at different starch concentrations is not well fitted by the calculations. In the case of WCS, the

spread in dependency on concentrations is better reflected by the model, but the drop sizes are generally over predicted even with the corrected calculation. Nevertheless the dependency of the measured drop size on ALR is qualitatively well reflected by the model in all cases.

Analysis of the model shows some possible reasons for the incorrect predictions: The first step is a simplistic geometrical model calculation of the ligament diameters and therefore depends neither on surface tension nor rheological properties. The calculated ligament diameter is dependent only on *ALR*. This step assumes filament breakup occurs directly upon exiting the nozzle exit orifice without significant conical expansion of the filament which is again dependent on the *ALR* and pressure of the fluids.

Lörcher [10] addressed another limitation of the model of *Lund et al.* that is likely to cause problems. The model of *Lund et al.* assumes the idealized case of a constant annular flow in the nozzle exit orifice, which is only valid for a small range of *ALR*. Below this range it is likely that plug or bubbly two-phase flow will occur, which will lead to unstable atomization conditions and are not considered in the used model. Above this *ALR* range spray instabilities may occur due to the high air flow causing an unstable annular flow and discontinuities of the filament sheaths.

To investigate the stability of the atomization process in this work, high speed video images of the near nozzle spray structure were evaluated. Sprays of CS with 4,5 wt% at *ALR* between 0,072 and 0,499 are shown in figures 3 to 5. At an *ALR* of 0,072 strong unsteadiness due to partial plug flow is clearly visible. With increasing *ALR* the spray structure becomes more stable and more homogenous so a stable annular flow in the nozzle exit orifice can be assumed at an *ALR* of 0,499. Figures 6 to 8 show sprays of CS at about the same *ALR* with a concentration from 3,5 wt.% to 5,5 wt.%. The spray structure changes from stable to unstable with increasing starch concentrations. This is due to the increase in viscosity with increasing starch concentration as listed in table 1. The change of rheological properties influences the *ALR* range for which a stable annular flow exists [11]. The selected high speed images show general trends also seen in other *ALR* ranges and starch concentrations – both for CS and WCS.

Figure 9 shows volumetric density distributions q_3 for CS spray with 4,5 wt.% and WCS spray with 2,5 wt.% at varying *ALR*. A systematic change in the volumetric density distributions is seen with variation in *ALR*. The tail above 100 µm is assumed to result from spray unsteadiness in the *ALR* range below the stable annular flow mentioned above. The increase of the main peak below 100 µm is assumed to correspond to the more stable annular flow caused by increasing *ALR*. The same trends are also found for other investigated starch concentrations.

As described above it is assumed that the main peak in the volumetric density distribution q_3 is associated with atomization due to annular flow. It can be characterized by a volumetric modal value, $x_{mod,3}$. As mentioned previously the model of *Lund et al.* is only valid for annular flow. Therefore the experimental modal value is compared to the calculated representative drop sizes and the experimental Sauter mean diameters in figure 10. Neither trends nor magnitudes of the modal value fit the calculated representative drop sizes. They are also in contrast to the experimental Sauter mean diameters. This finding is also valid for other starch concentrations. Therefore the comparison of calculated representative drop sizes and experimental modal value is not considered any further.

In summary, it can be conclusively stated that the *ALR* range considered in this investigation did cover unsteady atomization conditions at lower values. Despite this fact, the prediction of representative drop sizes compared to experimental Sauter mean diameters did not show an increased difference to the measured values in the range of unstable atomization. The trend of the drop sizes could be predicted for the complete *ALR* range of this investigation.

Several possible reasons for deviations between measured and calculated values have been discussed above. The investigation of the influence of the material properties during the breakup of the filament seems to be most promising. Another issue to be addressed is the correct definition of the material properties used when considering rheological properties of gelatinized starch suspensions as a fairly complex system. The mentioned issues are focus of current investigations.

Acknowledgement

This work has been carried out in cooperation of the Karlsruhe Institute of Technology (KIT), Section Food Process Engineering, and Purdue University, School of Mechanical Engineering / Maurice J. Zucrow Laboratories. The authors would like to thank the Institute of Mechanical Process Engineering and Mechanics of the KIT for supporting the rheological characterization. The work at the KIT has been carried out with financial support of the German Research Foundation (DFG) within the research program DFG-SPP 1423 “Prozess-Spray”.

Nomenclature

ALR	air-liquid mass ratio [-]
CS	corn starch
d	diameter [m]
q_3	volumetric density distribution [1/m]
x_{rep}	representative drop size [m]
$x_{1,2}$	Sauter mean diameter [m]
$x_{mod,3}$	volumetric modal value [m]
t_F	filament thickness [m]
v	velocity [m/s]
WCS	waxy corn starch
α	void fraction [-]
η	viscosity [Pa·s]
ρ	density [kg·m^{-3}]
σ	surface tension [N/m]

Subscripts

a	air
l	liquid
A	air core
L	ligament
O	orifice

References

[1] Sovani, S. D. et al., *Progress in Energy and Combustion Science* 27:483-521 (2001).
[2] Chawla, J. M., "Verfahren für die Zerstäubung von Flüssigkeiten oder für die Zerteilung von Gasen in kleine Blasen", DE2627880 C2 (1982).
[3] Lefebvre, A.H., *Atomization and Sprays*, Hemisphere Publishing Corporation, pp. 142-146
[4] Geckler, S. C. et al., *Journal of Fluid Engineering* 130:61303-61400 (2008).
[5] Lund, M. T. et al., *Atomization and Sprays* 3:77-89 (1993).
[6] Babinsky, E. et al., *Progress in Energy and Combustion Science*, 28:303-329 (2002).
[7] Qian, L. J. et. al., *Journal of Thermal Spray Technology* 19:586-601, 2010.
[8] Ishii, M., "One-dimensional drift-flux model and constitutive equations for relative motion between phases in various two-phase flow regimes", Argonne National Laboratory Report No. ANL-77-47
[9] Weber, C., *Zeitschrift für Angewandte Mathematik und Mechanik* 11:136-154 (1931)
[10] Lörcher, M., *Zerstäuben von zweiphasigen Gemischen aus Flüssigkeiten und Gasen*, VDI Verlag GmbH, 2003, pp. 107-109
[11] Chin, J. S. et al., *Journal of Engineering for Gas Turbines and Power-Transactions of the ASME* 117: 266-271, 1995.

Table 1. Material properties of the gelatinized starch suspensions used in the experiments.

Sample	**CS 3,5 wt.%**	**CS 4,5 wt.%**	**CS 5,5 wt.%**
viscosity η_L [Pa·s]	0,00362	0,00609	0,01368
surface tension σ [N/m]	0,07089	0,07299	0,07294
Sample	**WCS 2,0 wt.%**	**WCS 2,5 wt.%**	**WCS 3,0 wt.%**
complex viscosity $\lvert\eta_L^*\rvert$ [Pa·s]	0,1195	0,2755	1,4333
surface tension σ [N/m]	0,07390	0,07413	0,07428

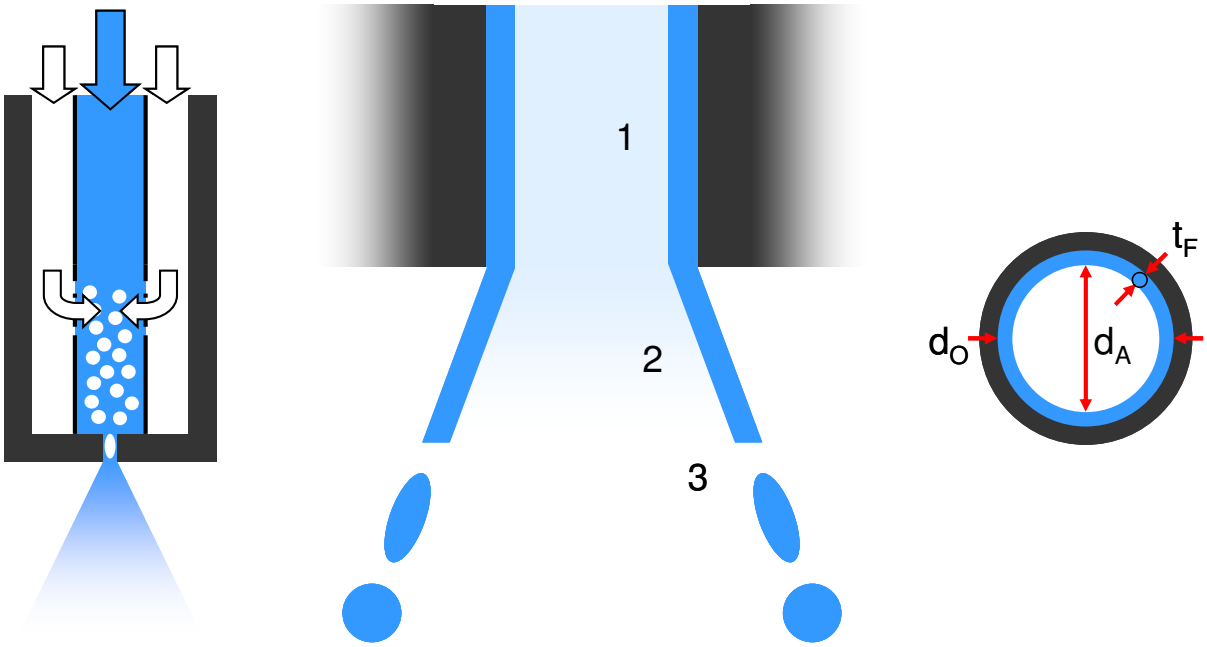

Figure 1. Scheme of effervescent atomization process; nozzle overview (*left*) with injection of gas (outside) into liquid (inside) prior to nozzle exit orifice; flow in nozzle exit orifice and near nozzle (*middle*) with annular flow and continuous liquid filament (1), break up of filament into ligament (2) and ligament break up into drop (3); cross section of annular flow in nozzle exit orifice (*right*) with nozzle diameter d_O, air core diameter d_A, thickness of filament t_F and sphere with diameter t_F inserted to determine number of resulting ligaments.

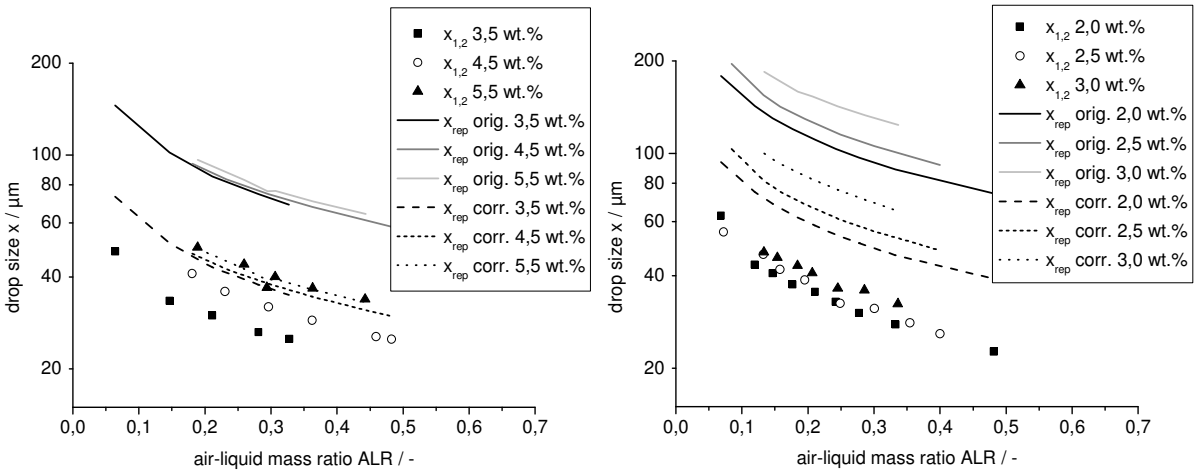

Figure 2. Experimental data (dots; $x_{1,2}$) and calculated drop sizes (lines; x_{rep} orig. → original calculation; x_{rep} corr. → corrected calculation) for CS (*left*) and WCS (*right*) with varying starch concentrations and *ALR*

Figure 3. High speed video images of the spray structure: CS 4,5 wt.%, *ALR* 0,072

Figure 4. High speed video images of the spray structure: CS 4,5 wt.%, *ALR* 0,228

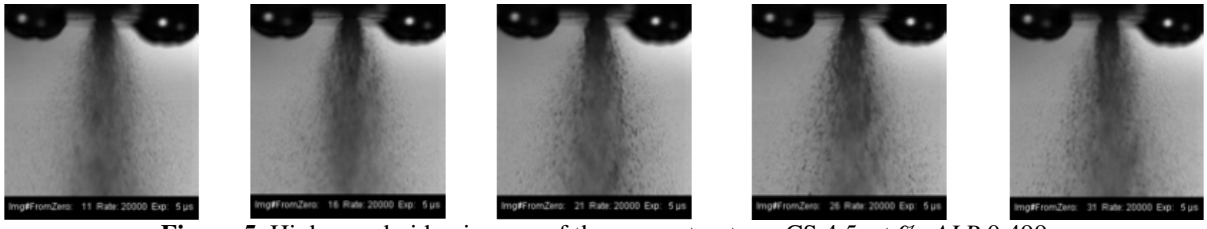

Figure 5. High speed video images of the spray structure: CS 4,5 wt.%, *ALR* 0,499

Figure 6. High speed video images of the spray structure: CS 3,5 wt.%, *ALR* 0,281

Figure 7. High speed video images of the spray structure: CS 4,5 wt.%, *ALR* 0,228

Figure 8. High speed video images of the spray structure: CS 5,5 wt.%, *ALR* 0,293

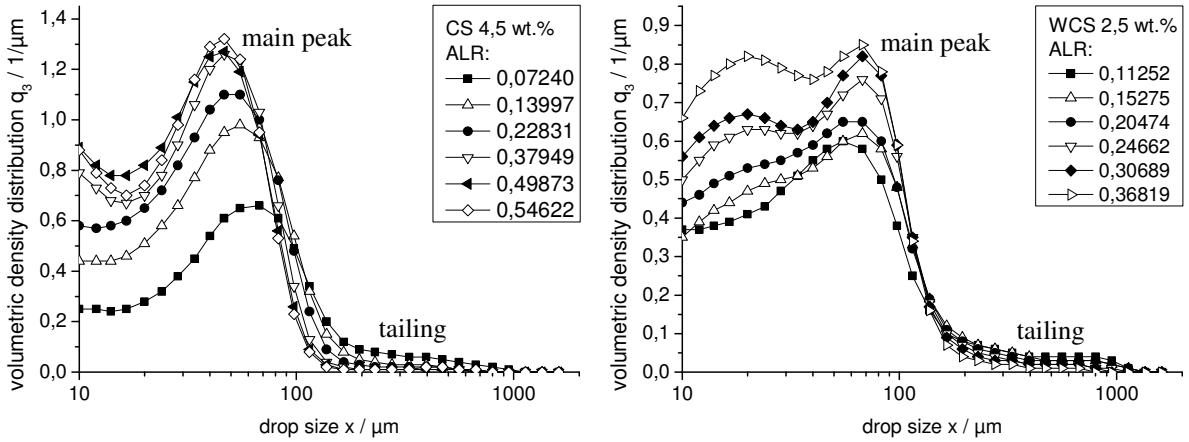

Figure 9. Volumetric density distribution q_3 of CS with 4,5 wt.% and WCS with 2,5 wt.% at varying *ALR*. A main peak below 100 µm and tailing above 100 µm can be seen.

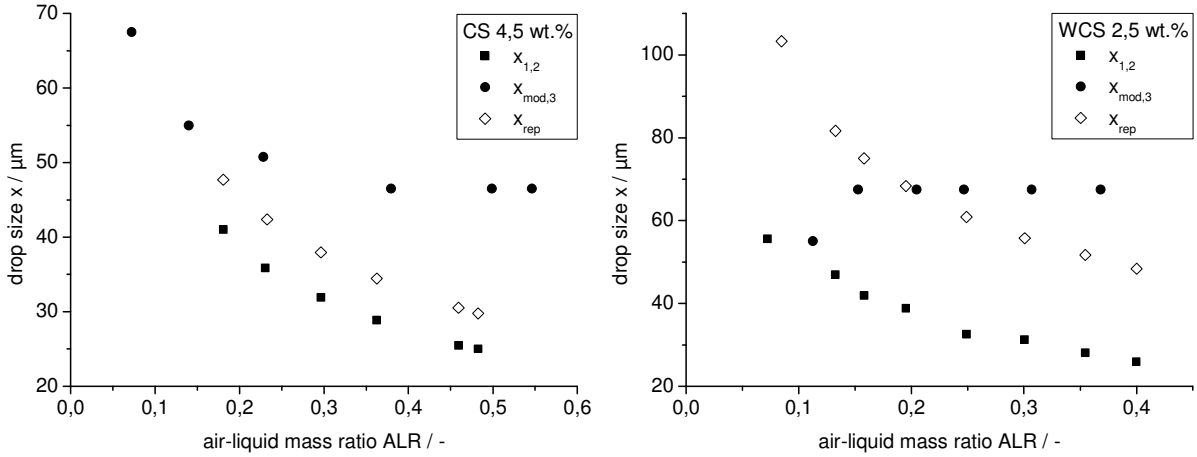

Figure 10. Calculated representative drop sizes x_{rep} compared to volumetric modal values $x_{mod,3}$ for CS with 4,5 wt.% and WCS with 2,5 wt.% at varying *ALR*.